

---

# No Train, all Gain: Self-Supervised Gradients Improve Deep Frozen Representations

---

Walter Simoncini<sup>1,\*</sup>   Spyros Gidaris<sup>2</sup>   Andrei Bursuc<sup>2</sup>   Yuki M. Asano<sup>1</sup>

<sup>1</sup> QUVA Lab, University of Amsterdam <sup>2</sup> valeo.ai, Paris, France

## Abstract

This paper introduces FUNGI, Features from UNsupervised GradIents, a method to enhance the features of vision encoders by leveraging self-supervised gradients. Our method is simple: given any pretrained model, we first compute gradients from various self-supervised objectives for each input. These are projected to a lower dimension and then concatenated with the model’s embedding. The resulting features are evaluated on k-nearest neighbor classification over 11 datasets from vision, 5 from natural language processing, and 2 from audio. Across backbones spanning various sizes and pretraining strategies, FUNGI features provide consistent performance improvements over the embeddings. We also show that using FUNGI features can benefit linear classification and image retrieval, and that they significantly improve the retrieval-based in-context scene understanding abilities of pretrained models, for example improving upon DINO by +17% for semantic segmentation – without any training. Code is available at <https://github.com/WalterSimoncini/fungivision>.

## 1 Introduction

The k-nearest neighbor algorithm (kNN) (Fix, 1985) is a fundamental non-parametric machine learning tool, and can be scaled to datasets with billion of examples thanks to advances in quantization (Jegou et al., 2010; Guo et al., 2020) and efficient GPU implementations (Johnson et al., 2019). This simple and versatile algorithm has shown potential in multiple applications well before deep neural networks became relevant (Efros & Leung, 1999; Hays & Efros, 2008; Torralba et al., 2008). Its recent applications include fast and robust image classification with Vision Transformers (Caron et al., 2021; Chen & He, 2021), unlabeled data selection (Yalniz et al., 2019), relevant text-retrieval (Lewis et al., 2020), and visual in-context learning (Balazevic et al., 2024), where a context of data samples with their annotations (e.g., a semantic segmentation map) are used to make dense predictions.

Devising powerful and expressive features for recognition and image understanding has a long history in computer vision. Feature engineering strategies range from simple local features (Lowe, 2004; Dalal & Triggs, 2005; Van De Sande et al., 2009) extracting gradient, boundary or color information, to various mid-level (Boureau et al., 2010) or global pooling (Oliva & Torralba, 2001; Sivic & Zisserman, 2003; Jégou et al., 2010) techniques. It is also possible to couple off-the-shelf pretrained backbones as feature extractors with such pooling strategies (Gong et al., 2014; Kulkarni et al., 2015; Gidaris et al., 2020) to improve performances. While these approaches demonstrate the utility of using a neural network’s learned embedding space, they still require specific expertise and tuning for each backbone and task with only limited guidance from the data itself.

---

\*Work partially done as an intern at valeo.ai. Datasets were solely downloaded and evaluated by the University of Amsterdam. [walter@ashita.nl](mailto:walter@ashita.nl)

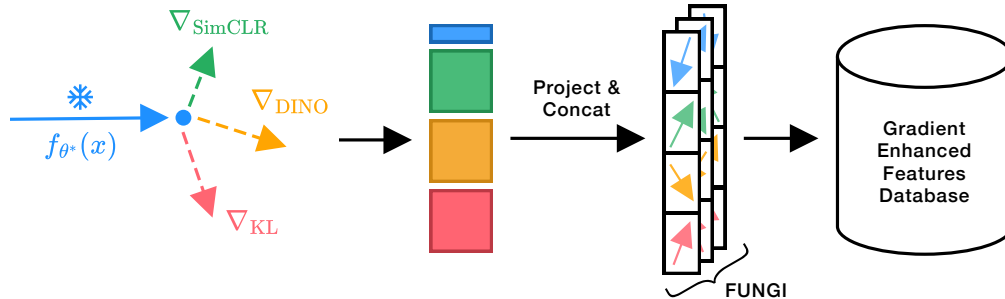


Figure 1: **Gradient-augmented features**: given a pretrained backbone  $f_{\theta^*}$  and its embeddings, we apply a family of SSL losses, extract their gradients, and project and concatenate them. These new features are used to build a  $k$ -nearest neighbor index, which can be used for classification or retrieval.

We depart from this line of work and aim to attain strong representations without training and feature engineering, yet still exploiting information cues from data. In particular, we suggest to enhance the neural network’s embeddings by incorporating FUNGI (Features from Unsupervised Gradients). FUNGI are obtained from self-supervised loss functions, as these do not require any human annotations and allow for a simple enhancement to embedding-only kNN. The losses are computed on top of pretrained backbones (with randomly initialized linear layers if needed), which permits our method to be “plug-and-play” and benefit from the diverse set of pretraining objectives put forth by the community.

We explore gradients from various learning objectives, such as contrastive learning (Chen et al., 2020a) and self-distillation (Caron et al., 2021) thereby integrating complementary information that mitigates the weaknesses of individual losses. The gradients are obtained from late hidden layers, making them computationally cheap. Finally, these are projected to smaller dimensions, and concatenated with the neural network embeddings, to yield new inputs to the classic kNN algorithm.

Using kNN with FUNGI can be regarded as a non-parametric transfer learning approach: the gradient information encodes first-order learning signals that are specific to the downstream data, yet no parameters need to be updated. Despite this simplicity, we achieve consistent performance improvements across multiple models and benchmarks.

Overall, our main contributions are summarized as follows:

- We introduce FUNGI, a novel method that combines neural network features and gradients to enhance representations for the  $k$ -nearest neighbor algorithm.
- We demonstrate that the gradients from self-supervised losses have predictive abilities and offer complementary information to model embeddings.
- We validate the generality and utility of our method by achieving consistent gains across 11 image, 5 text, and 2 audio classification benchmarks, plus 2 in-context image segmentation and 2 image retrieval tasks, utilizing a total of 16 backbones.

## 2 Related Work

**Fast Adaptation** There is a broad range of approaches to quickly adapt models to newly specified tasks and data. Inspired by early *learning-to-learn* work (Hochreiter et al., 2001), *meta-learning* methods (Finn et al., 2017; Nichol et al., 2018) learn to initialize the parameters of a learner such that it becomes faster to fine-tune with a small number of gradient steps and data. Alternative approaches leverage external memory modules to store relevant training samples to learn to match query examples (Santoro et al., 2016; Vinyals et al., 2016), learn to produce and compare class-based prototypes (Snell et al., 2017) or learn to generate the weights of a classifier (Gidaris & Komodakis, 2018) or even of an entire neural network (Bertinetto et al., 2016) from only a few labeled examples. The advent of Vision Transformers (Dosovitskiy et al., 2020) enable new parameter- and data-efficient strategies to adapt pretrained models through visual prompts (Jia et al., 2022) and in-context learning (Zhang et al., 2023). In contrast to this line of works, our method does not require specialized training and can be applied to any frozen pretrained backbone. FUNGI can also be related to test-time

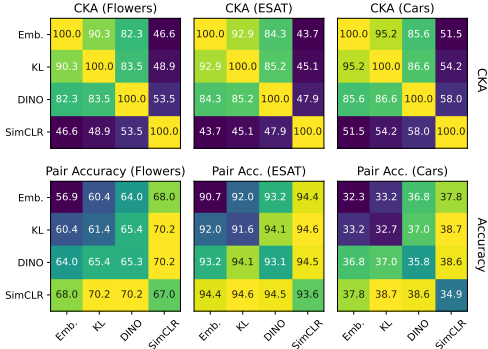


Figure 2: **Combining diverse features leads to large improvements.** The top plots display the pairwise CKA similarity between each pair of features, and the bottom shows the kNN accuracies for combining these.



Figure 3: **Gradients encode different information.** The plots show the delta in per-class accuracy of k-nearest neighbor models fitted with gradients from different objectives compared to a model fitted using the embeddings, indicated as “Emb.” in the plot.

training (Sun et al., 2020; Hardt & Sun, 2023), where the parameters of a predictive model are updated over test samples with a self-supervised objective to reduce the gap between the training and test distributions. While we also use self-supervised objectives and gradients, our approach does not update model parameters and is not limited to predictive models, as it can be applied to any task that can be solved with retrieval.

**Self-Supervised Learning Objectives** In recent years, self-supervised learning (SSL) has made tremendous progress in computer vision. SSL aims to learn good representations from unlabeled data by leveraging supervision from different signals in the data itself via pretext objectives, thus foregoing human supervision. Models pretrained with self-supervision are subsequently finetuned to downstream tasks of interest with few labeled samples. The crux of SSL is in the pretext learning objective. A wide and diverse collection of pretext objectives have been proposed in the community relying on contrastive learning (Chen et al., 2020a; He et al., 2020; Chen et al., 2020b), clustering (Caron et al., 2018; Asano et al., 2020; Caron et al., 2020), self-distillation (Caron et al., 2021; Grill et al., 2020; Chen & He, 2021; Gidaris et al., 2021), feature (Zhou et al., 2022; Assran et al., 2023) or input reconstruction (He et al., 2022). We hypothesize that the gradients induced by these objectives encapsulate different information from the input data, and that this information can be combined to produce more information-rich representations. Here, we do not use self-supervision in the usual way, *i.e.*, to pretrain an encoder, but rather focus on pretext objectives and data augmentation strategies to compute representations from a frozen pretrained model.

**Feature Engineering** A long-standing research area for pattern recognition and image understanding before the advent of deep neural networks that brought the paradigm of end-to-end representation learning. In contrast, classic feature extraction methods are devised without labeled data and often from only a few data samples. They range from local features, such as SIFT (Lowe, 2004), HOG (Dalal & Triggs, 2005), to global pooling, such as GIST (Oliva & Torralba, 2001), Bag-of-Visual-Words (Sivic & Zisserman, 2003), Fisher vectors (Perronnin et al., 2010), VLAD (Jégou et al., 2010), selective match kernels (Tolias et al., 2013), etc. These pooling strategies can be easily plugged to intermediate or output neural network activations (Gong et al., 2014; Kulkarni et al., 2015; Gidaris et al., 2020), harnessing data-driven learned representations. Other modern examples of feature engineering include kNN-prompting (Xu et al., 2023) that uses the next token probabilities of a language model to perform few shot nearest neighbor classification, LOST (Siméoni et al., 2021) which uses patch features from self-supervised vision transformers for object localization and FroFA (Bär et al., 2024), which applies data augmentation to deep features. FUNGI can also be seen as a form of feature engineering: by making use of different pretext tasks, we are able to extract multiple complementary features from a pretrained backbone.

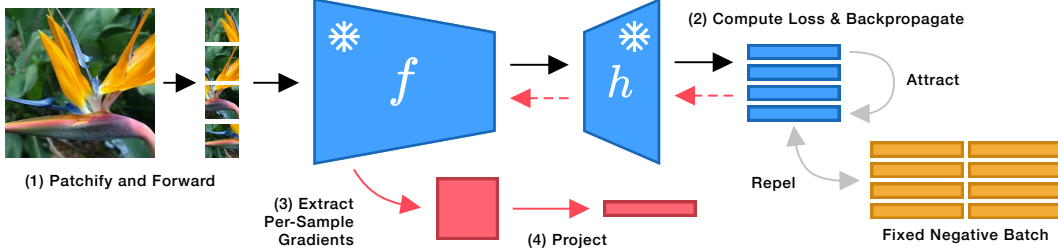


Figure 4: **Gradients extraction using a SimCLR loss.** Given a pretrained backbone  $f$  and a randomly initialized projection head  $h$ , we first patchify an image, obtain the latent representations of patches (1), calculate the SimCLR loss by maximizing the pairwise cosine similarity of patches, and minimizing their similarity to a fixed negatives batch and backpropagate (2), extract the per-sample gradients (3) and finally project the gradients to the same dimensionality as the embeddings (4).

### 3 What Gradients to Combine?

The core assumption of our method is that gradients encode complementary information to the model embeddings. We show that this holds in Figure 2, where we compare the centered kernel alignment (CKA) (Kornblith et al., 2019) score of different feature pairs to the accuracy in k-nearest neighbor classification of their combination. The plot shows that feature combinations always perform better than a single feature and that combining more diverse features leads to better downstream performance. We further highlight the difference between gradients and embeddings in Figure 3, which shows that performing k-nearest neighbor classification with gradients yields different predictions compared to the embeddings and that the per-class accuracy distribution changes across the type of gradient-features suggesting that they are complementary to both embeddings and each other.

## 4 Method

Our method, FUNGI, enhances k-nearest neighbor search by incorporating features from unsupervised gradients. We extract gradients from self-supervised loss functions, project them to smaller dimensions, and concatenate them with neural network embeddings. The extraction of self-supervised gradients is illustrated in Figure 4, while Figure 1 shows how FUNGI features are constructed.

**Definitions** Throughout this section, we define  $L_2$  normalization as  $z' = z/\|z\|_2$ , a vision backbone as  $f$ , a linear projection head as  $h$  and vectorization as  $\text{vec}(\cdot)$ .

### 4.1 FUNGI: Features from Unsupervised Gradients

**Gradients Extraction.** Given an arbitrary vision backbone  $f$ , which in our case is a vision transformer (ViT) (Dosovitskiy et al., 2020), we attach a randomly initialized linear projection head  $h$  and obtain a latent representation  $z = h(f'(x))$  of the input images, which we use to compute the loss for one of our self-supervised objectives. We then run backpropagation and extract the gradients with respect to the weights and biases of an arbitrary hidden linear layer within  $f$ . Unless specified otherwise, we use the attention output projection of the last transformer block as our gradient’s source.

**From Gradients to Retrieval-Friendly Features.** Gradients are high dimensional and thus impractical for nearest-neighbor retrieval due to speed and storage considerations and the curse of dimensionality. To tackle these issues, we downsample the gradients to the dimensionality of original model embeddings  $d$  using the random projections introduced by Achlioptas (2003). For this, we first vectorize the gradients by flattening them to a  $m$ -dimensional vector and then multiply them by a matrix  $R \in \{-1, 1\}^{d,m}$  whose entries are the realizations of a Bernoulli random variable with  $p = 0.5$ . The gradient  $g_\beta$  with respect to a loss  $\mathcal{L}_\beta$  is then defined as

$$g_\beta(x) = R \text{vec}(\nabla \mathcal{L}_\beta(x)). \quad (1)$$

**Combining with Embeddings** To produce our FUNGI features  $\phi$ , we concatenate one or more gradients to the model embeddings. As gradient magnitudes can vary widely across losses, and we

want gradients to be equally considered as the embeddings, we  $L_2$ -normalize each gradient, as well the embeddings and compute

$$\phi(x) = \text{cat} [g'_{\beta_1}(x), g'_{\beta_2}(x), \dots, f'(x)], \quad (2)$$

where `cat` denotes concatenation. Finally, we reduce the dimensionality of these combined features via PCA to a  $d$ -dimensional vector. This allows the combination of multiple losses at iso-storage cost. Our final FUNGI features for a sample  $x$  are thus obtained as:

$$\phi_{\text{PCA}}(x) = \text{PCA}_d(\phi(x)). \quad (3)$$

## 4.2 Self-Supervised Objectives

We consider losses representing three families of self-supervised objectives: DINO (Caron et al., 2021), SimCLR (Chen et al., 2020a) and a KL-divergence based loss inspired by the *out-of-distribution* detection literature (Huang et al., 2021). In this section we briefly describe the objectives and our adjustments to them, and in Appendix A.4, we also briefly discuss clustering and masked image modeling-based losses.

**DINO.** DINO is a distillation and implicit clustering-based learning method. We use the standard DINO loss, which, given an image, enforces global and local crop correspondence between teacher and student models using a cross-entropy loss. In our case, both models share the same parameters, but have independent heads  $h_s$  and  $h_t$  for student and teacher respectively, thus we have  $z_i = h_i(f'(x))$ ,  $i \in \{s, t\}$ . The DINO objective can be expressed as:

$$\mathcal{L}_{\text{DINO}} = \text{Cross-Entropy}(z_s, z_t). \quad (4)$$

**SimCLR.** SimCLR is a noise-contrastive method. Given a batch of images, SimCLR generates two views for each image and aims to minimize the distance between views belonging to the same image and maximize their distance to all other views. Instead, we generate a set of 49 overlapping patches for each image, which we call the positive set. This set is then contrasted against a fixed comparison batch of  $49 \times 256$  negative examples. Our objective is the expectation of the pair-wise InfoNCE (Oord et al., 2018) loss for each pair of positive views. If we define the positive set of latent view representations as  $Z$ , where  $z_i \in Z = h'(f(x_i))$  for a view  $x_i$ , and the comparison batch size as  $N$  the  $\mathcal{L}_{\text{SimCLR}}$  objective is then defined as:

$$\mathcal{L}_{\text{SimCLR}} = \mathbb{E}_{(z_i, z_j) \sim Z, z_i \neq z_j} [\ell_{z_i, z_j}] \quad \ell_{z_i, z_j} = -\log \frac{\exp(\text{sim}(z_i, z_j)/\tau)}{\sum_{k=1}^{49(N+1)} \mathbb{1}_{[k \neq i]} \exp(\text{sim}(z_i, z_k)/\tau)}. \quad (5)$$

**KL Divergence.** The KL objective is calculated as the KL divergence between the softmaxed logits of the latents and a uniform distribution  $\mathcal{U}$ :

$$\mathcal{L}_{\text{KL}} = \text{KL}(\text{softmax}(z) || \mathcal{U}). \quad (6)$$

We hypothesize two reasons as for why this loss produces predictive gradients: first, it receives a non-augmented image, with a higher signal-to-noise ratio compared to other objectives, and second, if we assume that similar images (*e.g.*, the ones that belong to the same class) produce similar activations, then maximizing their entropy by forcing the output distribution to match an uniform should produce similar intra-class gradients and help separability. This hypothesis is supported by the fact that while the KL gradients are discriminative, they have chance performance in other tasks, such as in-context scene understanding.

## 4.3 In-Context Scene Understanding

Balazevic et al. (2024) introduced a method for retrieval-based in-context scene understanding, where, for semantic segmentation, they first build a memory bank containing training image patches and their labels, and at test time, for each image patch, retrieve its nearest neighbors and use them to predict its label using an attention mechanism. Images are first resized to  $512 \times 512$ , and then encoded as a set of  $32^2 = 1024$  patch features using a ViT with patch size 16.

We enhance the patch features using SimCLR gradients, obtained by contrasting the input patch tokens against their nearest neighbors from a support index built with ScaNN (Guo et al., 2020). We use the reproduction of this evaluation protocol by Pariza et al. (2024) to run our experiments.

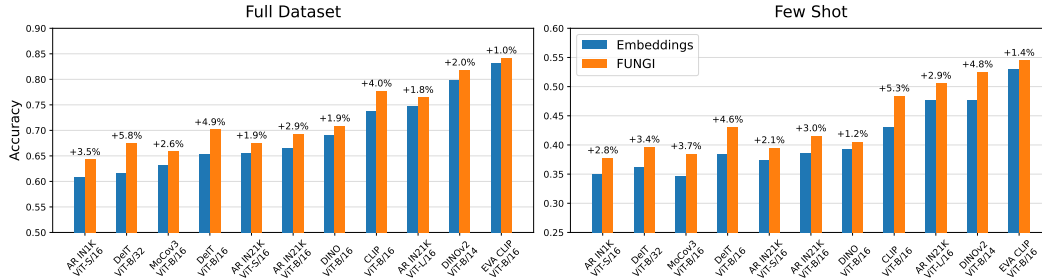


Figure 5: **FUNGI works across backbones.** Accuracy in  $k$ -nearest neighbor classification using embeddings and FUNGI features from various ViT backbones, both for full dataset and few shot setups, averaged over 11 datasets. For the FUNGI features we chose the best performing combination across datasets. “AR” indicates backbones trained with the AugReg strategy (Steiner et al., 2021).

Table 1: **FUNGI features are better on several datasets.** Accuracy of embeddings and FUNGI features in kNN classification over 11 datasets, for two AugReg (Dosovitskiy et al., 2020; Steiner et al., 2021) ViT-B/16 models from timm (Wightman, 2019) pretrained on IN1K and IN21K.

	Pretrain	Cars	CUB	DTD	ESAT	C100	C10	Pets	Food	IN1K	FGVC	Flowers	Mean
<b>Full dataset</b>													
Embeddings	IN1K	21.3	42.0	54.3	89.0	66.3	89.4	87.3	52.3	77.2	17.9	53.8	59.2
FUNGI	IN1K	<b>27.2</b>	<b>50.1</b>	<b>58.6</b>	<b>93.4</b>	<b>69.7</b>	<b>90.7</b>	<b>89.5</b>	<b>58.9</b>	<b>78.8</b>	<b>21.4</b>	<b>61.6</b>	<b>63.6</b> $\uparrow 4.4$
Embeddings	IN21K	21.0	74.0	58.4	91.8	58.4	82.9	83.6	70.6	72.1	23.0	95.0	66.4
FUNGI	IN21K	<b>25.1</b>	<b>74.2</b>	<b>65.0</b>	<b>94.7</b>	<b>63.5</b>	<b>85.7</b>	<b>85.7</b>	<b>73.4</b>	<b>74.5</b>	<b>24.3</b>	<b>96.6</b>	<b>69.3</b> $\uparrow 2.9$
<b>5-Shot</b>													
Embeddings	IN1K	9.4	23.7	32.5	38.6	36.9	48.8	57.5	20.1	55.7	8.3	41.2	33.9
FUNGI	IN1K	<b>11.4</b>	<b>26.6</b>	<b>33.9</b>	<b>42.2</b>	<b>38.6</b>	<b>50.2</b>	<b>59.4</b>	<b>24.1</b>	<b>58.6</b>	<b>9.2</b>	<b>49.8</b>	<b>36.7</b> $\uparrow 2.8$
Features	IN21K	7.6	<b>50.0</b>	33.7	47.7	23.2	39.7	<b>53.3</b>	32.0	40.3	10.7	<b>86.2</b>	38.6
FUNGI	IN21K	<b>9.2</b>	48.5	<b>36.3</b>	<b>54.5</b>	<b>28.2</b>	<b>41.7</b>	51.0	<b>37.8</b>	<b>45.4</b>	<b>12.2</b>	85.8	<b>41.0</b> $\uparrow 2.4$

## 5 Experiments

In this section, we evaluate the performance of FUNGI in  $k$ -nearest neighbor image and text classification and retrieval-based in-context scene understanding. Further experiments, including image retrieval and audio classification, are provided in Appendix A.

### 5.1 Image Classification

Following Caron et al. (2021), we evaluate our FUNGI features using the task of kNN classification. To show the generalizability of our method, we evaluate our features across ViT backbones (Dosovitskiy et al., 2020) with varying model sizes and pretraining strategies, including both supervised and self-supervised methods.

We conduct our experiments on 11 diverse downstream datasets, described in Appendix C. Unless otherwise specified, we report the average accuracy across these datasets. We evaluate our features using the kNN implementation of scikit-learn (Pedregosa et al., 2011) with majority voting over 20 neighbors, for full dataset and few shot scenarios, the latter using five examples per class, to analyze the efficacy of our approach in low-data scenarios.

Our results, presented in Figure 5, show that FUNGI consistently improves the kNN performance of all ViT models, regardless of model size or pretraining strategy, both for the full dataset and in few shot scenarios.

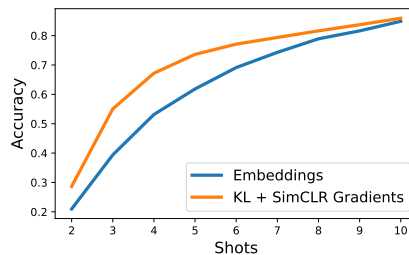


Figure 6: **Better data-efficiency.** kNN accuracy of embeddings and FUNGI (using only KL and SimCLR gradients) on ImageNet-100 using a DeiT-B/16 backbone when only  $k$  shots are used.

Table 2: **Performance improves as more gradients are used.** Accuracy in image classification using kNN with embeddings and FUNGI, averaged across 11 datasets for 7 backbones, for standard and few shot setups. Results for additional backbones are shown in Table 8. “K”, “D” and “S” stand for KL, DINO and SimCLR, respectively.

	DINOv2 ViT-B/14	DINO ViT-B/16	DeiT ViT-B/16	MoCov3 ViT-B/16	DeiT ViT-B/32	AugReg IN1K ViT-S/16	AugReg IN1K ViT-B/16
<b>Full Dataset</b>							
Embeddings	79.9	69.0	65.3	63.2	61.7	60.8	59.2
+ K	80.6 $\uparrow$ 0.7	69.4 $\uparrow$ 0.4	66.3 $\uparrow$ 1.0	63.4 $\uparrow$ 0.2	63.3 $\uparrow$ 1.6	60.3 $\downarrow$ 0.5	58.9 $\downarrow$ 0.3
+ K + D	81.3 $\uparrow$ 1.4	70.1 $\uparrow$ 1.1	68.1 $\uparrow$ 2.8	64.7 $\uparrow$ 1.5	65.7 $\uparrow$ 4.0	62.6 $\uparrow$ 1.8	61.1 $\uparrow$ 1.9
+ K + D + S	<b>81.7 <math>\uparrow</math>1.8</b>	<b>70.9 <math>\uparrow</math>1.9</b>	<b>70.1 <math>\uparrow</math>4.8</b>	<b>65.8 <math>\uparrow</math>2.6</b>	<b>67.3 <math>\uparrow</math>5.6</b>	<b>64.3 <math>\uparrow</math>3.5</b>	<b>63.6 <math>\uparrow</math>4.4</b>
<b>Few Shot</b>							
Features	47.6	39.3	38.4	34.7	36.2	34.9	33.9
+ K	48.1 $\uparrow$ 0.5	39.4 $\uparrow$ 0.1	38.7 $\uparrow$ 0.3	35.8 $\uparrow$ 1.1	36.6 $\uparrow$ 0.4	34.2 $\downarrow$ 0.7	33.5 $\downarrow$ 0.4
+ K + D	49.1 $\uparrow$ 1.5	39.7 $\uparrow$ 0.4	39.1 $\uparrow$ 0.7	36.6 $\uparrow$ 1.9	37.6 $\uparrow$ 1.4	35.0 $\uparrow$ 0.1	34.5 $\uparrow$ 0.6
+ K + D + S	<b>50.3 <math>\uparrow</math>2.7</b>	<b>40.5 <math>\uparrow</math>1.2</b>	<b>41.1 <math>\uparrow</math>2.7</b>	<b>38.2 <math>\uparrow</math>3.5</b>	<b>39.0 <math>\uparrow</math>2.8</b>	<b>36.5 <math>\uparrow</math>1.6</b>	<b>36.7 <math>\uparrow</math>2.8</b>

Table 3: **FUNGI features improve in-context semantic segmentation.** mIoU for retrieval-based semantic segmentation on Pascal VOC 2012, comparing a DINO baseline against FUNGI features and the self-supervised HummingBird model. Results from Balazevic et al. (2024) are marked with †. We resize each image to  $512 \times 512$  and extract  $32^2 = 1024$  patch features.

Backbone	Features	Memory Bank Size		
		$1024 \times 10^2$	$1024 \times 10^3$	$1024 \times 10^4$
DINO ViT-S/16	Embeddings	37.2	43.1	46.6
DINO ViT-S/16	FUNGI	<b>50.7 <math>\uparrow</math>13.5</b>	<b>56.3 <math>\uparrow</math>13.2</b>	<b>58.0 <math>\uparrow</math>11.4</b>
DINO ViT-B/16	Embeddings	44.9	50.8	55.7
DINO ViT-B/16	FUNGI	<b>62.1 <math>\uparrow</math>17.2</b>	<b>66.1 <math>\uparrow</math>15.3</b>	<b>67.0 <math>\uparrow</math>11.3</b>
HummingBird ViT-B/16†	Embeddings	-	-	<b>70.5</b>



Figure 7: **FUNGI produces sharper and more complete segmentation masks.** Segmentation masks produced via nearest neighbor retrieval using DINO features (left), FUNGI (center) and the ground truth (right). Both methods use a memory bank of  $1024 \times 10^4$  patches.

We further investigate data-efficient settings in Figure 6, where FUNGI shows a significant improvement when 3 to 6 shots are used, highlighting the potential of FUNGI in low-data regimes.

In Table 1, we show that, with some exceptions, FUNGI provides consistent improvements across datasets for two AugReg (Steiner et al., 2021) ViT-B/16 backbones, pretrained on IN1K and IN21K, with FUNGI providing better results on the former. We further discuss these results in Section 6.

Lastly, in Table 2 we show that performance improves as more gradients from different self-supervised objectives are used.

## 5.2 In-Context Scene Understanding

In this section, we assess the effectiveness of our approach in the task of retrieval-based semantic segmentation on Pascal VOC 2012 (Everingham et al., 2010) and ADE20K (Zhou et al., 2019, 2017). We use the trainaug and train splits to build the memory banks for VOC and ADE20K, respectively, and report the mean intersection over union (mIoU) on the validation set.

We apply FUNGI to the DINO ViT-S/16 and ViT-B/16 models. Our results, presented in Table 3 and Table 7, demonstrate that FUNGI significantly enhances DINO’s performance across all memory

Table 4: **Data-efficient semantic segmentation.** mIoU scores for data-efficient retrieval-based semantic segmentation on Pascal VOC 2012 and ADE20K, using DINO backbones and their FUNGI features and embeddings. We also compare FUNGI to end-to-end fine-tuning and find our method to perform best for VOC. Results from Balazevic et al. (2024) are marked with ‡.

		Dataset Size				
		Pascal VOC		ADE20K		
Backbone	Features	Decoder	1/128 ( $n = 83$ )	1/64 ( $n = 165$ )	1/128 ( $n = 158$ )	1/64 ( $n = 316$ )
ViT-B/16‡	-	E2E FT	36.1	44.3	<b>11.7</b>	<b>14.4</b>
ViT-S/16	Emb.	NN	26.3	31.8	8.8	10.0
ViT-S/16	FUNGI	NN	<b>29.1</b> †2.8	<b>34.0</b> †2.2	<b>10.2</b> †1.4	<b>12.3</b> †2.3
ViT-B/16	Emb.	NN	32.2	39.0	9.3	11.3
ViT-B/16	FUNGI	NN	<b>38.0</b> †5.8	<b>46.8</b> †7.8	<b>11.7</b> †2.4	<b>13.7</b> †2.4

Table 5: **FUNGI features are useful for the text modality.** Top-1 accuracy in kNN text classification for the full dataset and few shot setups. “K” and “S” stand for KL and SimCLR, respectively.

	TREC		Banking-77		SST (Fine Grained)		AG News		Tweet-Eval	
	Full	5-shot	Full	5-shot	Full	5-shot	Full	10-shot	Full	5-shot
<b>BERT Base</b>										
Features	83.6	20.0	55.4	14.5	40.0	20.4	88.8	45.8	23.8	13.6
+ K	85.6 †2.0	<b>27.6</b> †7.6	67.1 †11.7	22.2 †7.7	40.7 †0.7	<b>23.2</b> †2.8	<b>91.0</b> †2.2	61.4 †15.6	24.4 †0.6	13.8 †0.2
+ K + S	<b>86.8</b> †3.2	23.0 †3.0	<b>67.9</b> †12.5	<b>23.8</b> †9.3	<b>41.8</b> †1.8	18.4 †2.0	89.6 †0.8	<b>61.9</b> †16.1	<b>24.8</b> †1.0	<b>14.5</b> †0.9
<b>T5 Small</b>										
Features	<b>88.6</b>	<b>25.6</b>	29.7	5.2	30.0	<b>25.9</b>	71.8	37.4	23.4	8.4
+ K	<b>88.6</b>	23.6 †2.0	<b>33.3</b> †3.6	5.6 †0.4	<b>32.7</b> †2.7	24.1 †1.8	74.3 †2.5	40.6 †3.2	24.2 †0.8	9.5 †1.1
+ K + S	88.4 †0.2	23.6 †2.0	29.1 †0.6	<b>6.1</b> †0.9	32.0 †2.0	24.2 †1.7	<b>74.8</b> †3.0	<b>41.0</b> †3.6	<b>24.4</b> †1.0	<b>9.9</b> †1.5

bank sizes, with the most substantial improvements observed in smaller memory banks for VOC. Qualitatively, FUNGI produces sharper and more complete segmentation masks, as shown in Figure 7. Notably, the DINO ViT-B/16 model, when enhanced with our FUNGI approach, achieves competitive results against the current state-of-the-art HummingBird model (Balazevic et al., 2024), with a difference of only 3.5% on VOC and 3.1% on ADE20K, **without** any training. This is a particularly promising result, as HummingBird employs a self-supervised pretraining strategy that is specialized for retrieval-based dense prediction tasks, which are the focus of our evaluation in this study.

In addition, we evaluate the efficacy of FUNGI in a data-efficient setup, and report the results in Table 4. Our findings indicate that our method outperforms DINO in this scenario, even when compared to end-to-end fine-tuning of DINO on the downstream task for Pascal VOC.

### 5.3 Other Modalities

**Natural language.** We use five datasets, described in Appendix C, and two transformer language models: BERT base uncased (Devlin et al., 2018) and T5-small (Raffel et al., 2020). We use the  $\mathcal{L}_{\text{KL}}$  and  $\mathcal{L}_{\text{SimCLR}}$  losses and obtain the SimCLR views by randomly deleting words with a 10% probability. The results are presented in Table 5, and show that FUNGI achieves improvements in the text domain. However, SimCLR gradients struggle with some datasets. Different data augmentation strategies, such as back-translation (Sennrich et al., 2016), or language-specific self-supervised losses, *e.g.*, masked language modeling (Devlin et al., 2018), may yield more discriminative gradients. We leave this investigation for future work.

**Audio.** We demonstrate gains for the audio modality in Table 11, where we improve the ESC-50 kNN classification accuracy from 42.8% to 47.0% and SpeechCommands from 27.4% to 29.9% with an SSAST backbone (Gong et al., 2022). Further details are provided in Appendix A.2.

### 5.4 Ablation Studies

**Projection head.** To compute our self-supervised losses, we first  $L_2$ -normalize the model embeddings (except for SimCLR) and then project them using a randomly initialized linear head. We

Table 6: **Impact of the projection head configuration.** Top-1 accuracy of gradients on ImageNet-100 in k-nearest neighbor classification versus the projection head configuration for KL, DINO and SimCLR gradients. “norm” indicates whether the features are  $L_2$ -normalized before being projected. As features are always  $L_2$ -normalized for the SimCLR objective, the “empty” head configuration is not applicable. The default setup is marked in cyan .

$\nabla_{\text{KL}}$			$\nabla_{\text{DINO}}$			$\nabla_{\text{SimCLR}}$		
Norm	Projection	Acc.	Norm	Projection	Acc.	Norm	Projection	Acc.
		88.3			79.3			N/A
✓		87.3	✓		87.8	✓		88.7
	✓	88.8		✓	84.7		✓	<b>88.8</b>
✓	✓	<b>89.1</b>	✓	✓	<b>90.1</b>	✓	✓	88.7

motivate this choice empirically by ablating these components, and the results in Table 6 show that this configuration produces the most predictive gradients for ImageNet-100.

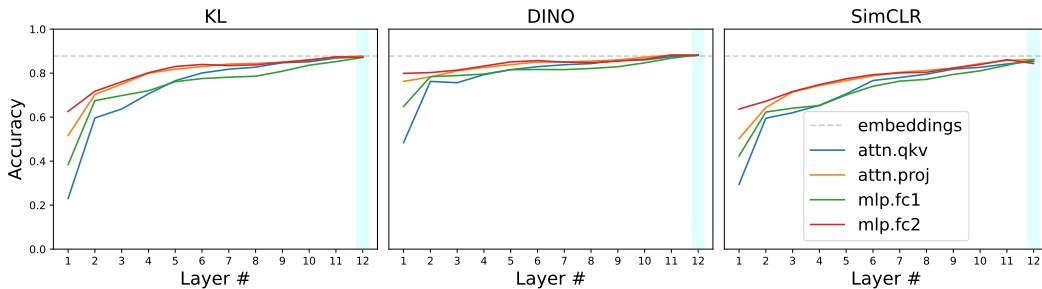


Figure 8: **Gradients from deeper layers are more predictive.** Top-1 accuracy of gradients obtained from every layer of a supervised DeiT ViT-B/16 in k-nearest neighbor classification on ImageNet-100 for the KL, DINO, and SimCLR objectives. The default setup (last layers) is marked in cyan .

**Gradients source layer.** Throughout the paper, we extract gradients from the self-attention output projection of the last transformer block. Intuitively, deeper layers provide more predictive features, and thus, their gradient should display the same behavior. This assumption is confirmed by our results in Figure 8, where, for all losses, deeper layers consistently produce more predictive gradients. Regarding the choice of layer within a transformer block, for shallower blocks, the second MLP layer is significantly more predictive, but the performance gap becomes insignificant as we move towards deeper blocks, favoring (by a small margin) the attention output projection. This layer is also more memory efficient, as it uses fewer parameters compared to other layers.

## 6 Discussion and Conclusion

**Broader impact.** Our method improves the features used for the kNN algorithm. As such, it is a fundamental contribution to Machine Learning. Given the ubiquitous use of kNN, our method could have positive consequences, such as improving reliability and factuality in Retrieval Augmented Generation (RAG) systems, where Language Models are grounded in retrieved pieces of text before generating an answer. We do not foresee any direct negative consequence caused by our method.

**Impact of pretraining dataset.** Our method works with various backbones, model sizes, and pretraining strategies. However, we have observed that the benefits diminish as the size of the pretraining dataset increases: in Table 1, FUNGI provides a smaller relative improvements on a backbone pretrained with IN21K compared to one pretrained on IN1K, and similarly, in Table 14 the relative improvement over EVA-CLIP (Sun et al., 2023) is smaller compared to CLIP (Radford et al., 2021), as they are pretrained on 2B and 400M text-image pairs respectively.

**Computational efficiency.** Computing FUNGI features introduces an overhead, which we measure in Table 22 by comparing the throughput of a DeiT ViT-B/16 when extracting gradients and embeddings. The DINO and SimCLR losses have the largest overhead, as they forward 12 and 49 views per

image, respectively. As shown in Appendix B.1, this number can be reduced, at a performance cost. However, thanks to our dimensionality reduction, the speed of kNN retrieval is not impacted.

## 7 Conclusion

We have shown that gradients from self-supervised objectives have predictive abilities and encode complementary information to the model embeddings. Building on those findings, we introduced FUNGI, which effectively combines embeddings and gradients into powerful features for retrieval-based tasks. Specifically, we have shown that FUNGI enhance the performance of kNN-based image and text classification across models, pretraining strategies, and downstream datasets, both for full dataset and few shot setups. Moreover, we have shown that FUNGI significantly boost the performance of DINO features for retrieval-based semantic segmentation tasks.

**Acknowledgements.** We acknowledge the use of the Dutch national supercomputer Snellius for running the experiments presented in this paper.

## References

- Dimitris Achlioptas. Database-friendly random projections: Johnson-lindenstrauss with binary coins. *JCSS*, 2003. 4
- Yuki M. Asano, Christian Rupprecht, and Andrea Vedaldi. Self-labelling via simultaneous clustering and representation learning. In *ICLR*, 2020. 3
- Mahmoud Assran, Quentin Duval, Ishan Misra, Piotr Bojanowski, Pascal Vincent, Michael Rabbat, Yann LeCun, and Nicolas Ballas. Self-supervised learning from images with a joint-embedding predictive architecture. In *ICCV*, 2023. 3
- Ivana Balazevic, David Steiner, Nikhil Parthasarathy, Relja Arandjelović, and Olivier Henaff. Towards in-context scene understanding. *NeurIPS*, 2024. 1, 5, 7, 8, 16, 20, 21
- Andreas Bär, Neil Houlsby, Mostafa Dehghani, and Manoj Kumar. Frozen feature augmentation for few-shot image classification. *arXiv preprint arXiv:2403.10519*, 2024. 3
- Francesco Barbieri, Jose Camacho-Collados, Francesco Ronzano, Luis Espinosa-Anke, Miguel Ballesteros, Valerio Basile, Viviana Patti, and Horacio Saggion. Semeval 2018 task 2: Multilingual emoji prediction. In *IWSE*, 2018. 23
- Francesco Barbieri, Jose Camacho-Collados, Luis Espinosa Anke, and Leonardo Neves. TweetEval: Unified benchmark and comparative evaluation for tweet classification. In *EMNLP*, 2020. 23
- Luca Bertinetto, João F Henriques, Jack Valmadre, Philip Torr, and Andrea Vedaldi. Learning feed-forward one-shot learners. In *NeurIPS*, 2016. 2
- Lukas Bossard, Matthieu Guillaumin, and Luc Van Gool. Food-101—mining discriminative components with random forests. In *ECCV*, 2014. 22, 23
- Y-Lan Boureau, Francis Bach, Yann LeCun, and Jean Ponce. Learning mid-level features for recognition. In *CVPR*, 2010. 1
- Mathilde Caron, Piotr Bojanowski, Armand Joulin, and Matthijs Douze. Deep clustering for unsupervised learning of visual features. In *ECCV*, 2018. 3, 18
- Mathilde Caron, Ishan Misra, Julien Mairal, Priya Goyal, Piotr Bojanowski, and Armand Joulin. Unsupervised learning of visual features by contrasting cluster assignments. *NeurIPS*, 2020. 3
- Mathilde Caron, Hugo Touvron, Ishan Misra, Hervé Jégou, Julien Mairal, Piotr Bojanowski, and Armand Joulin. Emerging properties in self-supervised vision transformers. In *ICCV*, 2021. 1, 2, 3, 5, 6, 24
- Iñigo Casanueva, Tadas Temčinas, Daniela Gerz, Matthew Henderson, and Ivan Vulić. Efficient intent detection with dual sentence encoders. *arXiv preprint arXiv:2003.04807*, 2020. 22, 23

- Ting Chen, Simon Kornblith, Mohammad Norouzi, and Geoffrey Hinton. A simple framework for contrastive learning of visual representations. In *ICML*, 2020a. 2, 3, 5
- Xinlei Chen and Kaiming He. Exploring simple siamese representation learning. In *CVPR*, 2021. 1, 3
- Xinlei Chen, Haoqi Fan, Ross Girshick, and Kaiming He. Improved baselines with momentum contrastive learning. *arXiv preprint arXiv:2003.04297*, 2020b. 3
- Xinlei Chen, Saining Xie, and Kaiming He. An empirical study of training self-supervised vision transformers. In *ICCV*, 2021. 24
- Mircea Cimpoi, Subhransu Maji, Iasonas Kokkinos, Sammy Mohamed, and Andrea Vedaldi. Describing textures in the wild. In *CVPR*, 2014. 22, 23
- Navneet Dalal and Bill Triggs. Histograms of oriented gradients for human detection. In *CVPR*, 2005. 1, 3
- Jacob Devlin, Ming-Wei Chang, Kenton Lee, and Kristina Toutanova. Bert: Pre-training of deep bidirectional transformers for language understanding. *arXiv preprint arXiv:1810.04805*, 2018. 8, 24
- Alexey Dosovitskiy, Lucas Beyer, Alexander Kolesnikov, Dirk Weissenborn, Xiaohua Zhai, Thomas Unterthiner, Mostafa Dehghani, Matthias Minderer, Georg Heigold, Sylvain Gelly, et al. An image is worth 16x16 words: Transformers for image recognition at scale. *arXiv preprint arXiv:2010.11929*, 2020. 2, 4, 6
- Alexei A Efros and Thomas K Leung. Texture synthesis by non-parametric sampling. In *ICCV*, 1999. 1
- M. Everingham, L. Van Gool, C. K. I. Williams, J. Winn, and A. Zisserman. The pascal visual object classes (voc) challenge. *IJCV*, 2010. 7
- Chelsea Finn, Pieter Abbeel, and Sergey Levine. Model-agnostic meta-learning for fast adaptation of deep networks. In *ICML*, 2017. 2
- Evelyn Fix. *Discriminatory analysis: nonparametric discrimination, consistency properties*, volume 1. USAF school of Aviation Medicine, 1985. 1
- Spyros Gidaris and Nikos Komodakis. Dynamic few-shot visual learning without forgetting. In *CVPR*, 2018. 2
- Spyros Gidaris, Andrei Bursuc, Nikos Komodakis, Patrick Pérez, and Matthieu Cord. Learning representations by predicting bags of visual words. In *CVPR*, 2020. 1, 3
- Spyros Gidaris, Andrei Bursuc, Gilles Puy, Nikos Komodakis, Matthieu Cord, and Patrick Pérez. Obow: Online bag-of-visual-words generation for self-supervised learning. In *CVPR*, 2021. 3
- Yuan Gong, Yu-An Chung, and James Glass. AST: Audio Spectrogram Transformer. In *Proc. Interspeech 2021*, pp. 571–575, 2021. doi: 10.21437/Interspeech.2021-698. 17, 18, 24
- Yuan Gong, Cheng-I Lai, Yu-An Chung, and James Glass. Ssast: Self-supervised audio spectrogram transformer. In *Proceedings of the AAAI Conference on Artificial Intelligence*, volume 36, pp. 10699–10709, 2022. 8, 17, 18, 24
- Yunchao Gong, Liwei Wang, Ruiqi Guo, and Svetlana Lazebnik. Multi-scale orderless pooling of deep convolutional activation features. In *ECCV*, 2014. 1, 3
- Jean-Bastien Grill, Florian Strub, Florent Altché, Corentin Tallec, Pierre Richemond, Elena Buchatskaya, Carl Doersch, Bernardo Avila Pires, Zhaohan Guo, Mohammad Gheshlaghi Azar, et al. Bootstrap your own latent—a new approach to self-supervised learning. In *NeurIPS*, 2020. 3
- Antonio Gulli. Ag’s corpus of news articles. [http://groups.di.unipi.it/~gulli/AG\\_corpus\\_of\\_news\\_articles.html](http://groups.di.unipi.it/~gulli/AG_corpus_of_news_articles.html), 2005. Accessed: 2020-05-21. 23

- Ruiqi Guo, Philip Sun, Erik Lindgren, Quan Geng, David Simcha, Felix Chern, and Sanjiv Kumar. Accelerating large-scale inference with anisotropic vector quantization. In *ICML*, 2020. [1](#), [5](#), [21](#)
- Moritz Hardt and Yu Sun. Test-time training on nearest neighbors for large language models. *arXiv preprint arXiv:2305.18466*, 2023. [3](#)
- James Hays and Alexei A Efros. Im2gps: estimating geographic information from a single image. In *CVPR*, 2008. [1](#)
- Kaiming He, Haoqi Fan, Yuxin Wu, Saining Xie, and Ross Girshick. Momentum contrast for unsupervised visual representation learning. In *CVPR*, 2020. [3](#)
- Kaiming He, Xinlei Chen, Saining Xie, Yanghao Li, Piotr Dollár, and Ross Girshick. Masked autoencoders are scalable vision learners. In *CVPR*, 2022. [3](#), [16](#), [24](#)
- Patrick Helber, Benjamin Bischke, Andreas Dengel, and Damian Borth. Eurosat: A novel dataset and deep learning benchmark for land use and land cover classification. *JST-AEORS*, 2019. [22](#), [23](#)
- Sepp Hochreiter, A Steven Younger, and Peter R Conwell. Learning to learn using gradient descent. In *ICANN*, 2001. [2](#)
- Rui Huang, Andrew Geng, and Yixuan Li. On the importance of gradients for detecting distributional shifts in the wild. *NeurIPS*, 2021. [5](#)
- Herve Jegou, Matthijs Douze, and Cordelia Schmid. Product quantization for nearest neighbor search. *TPAMI*, 2010. [1](#)
- Hervé Jégou, Matthijs Douze, Cordelia Schmid, and Patrick Pérez. Aggregating local descriptors into a compact image representation. In *CVPR*, 2010. [1](#), [3](#)
- Menglin Jia, Luming Tang, Bor-Chun Chen, Claire Cardie, Serge Belongie, Bharath Hariharan, and Ser-Nam Lim. Visual prompt tuning. In *ECCV*, 2022. [2](#)
- Jeff Johnson, Matthijs Douze, and Hervé Jégou. Billion-scale similarity search with gpus. *TBD*, 2019. [1](#)
- Simon Kornblith, Mohammad Norouzi, Honglak Lee, and Geoffrey Hinton. Similarity of neural network representations revisited. In *ICML*, 2019. [4](#)
- Jonathan Krause, Jia Deng, Michael Stark, and Li Fei-Fei. Collecting a large-scale dataset of fine-grained cars. 2013. [22](#), [23](#)
- Alex Krizhevsky, Geoffrey Hinton, et al. Learning multiple layers of features from tiny images. 2009. [22](#), [23](#)
- Praveen Kulkarni, Joaquin Zepeda, Frederic Jurie, Patrick Perez, and Louis Chevallier. Hybrid multi-layer deep cnn/aggregator feature for image classification. In *ICASSP*, 2015. [1](#), [3](#)
- Patrick Lewis, Ethan Perez, Aleksandra Piktus, Fabio Petroni, Vladimir Karpukhin, Naman Goyal, Heinrich Küttler, Mike Lewis, Wen-tau Yih, Tim Rocktäschel, et al. Retrieval-augmented generation for knowledge-intensive nlp tasks. In *NeurIPS*, 2020. [1](#)
- Xin Li and Dan Roth. Learning question classifiers. In *COLING*, 2002. [22](#), [23](#)
- David G Lowe. Distinctive image features from scale-invariant keypoints. *IJCV*, 2004. [1](#), [3](#)
- Julien Mairal. Cyanure: An open-source toolbox for empirical risk minimization for python, c++, and soon more. *arXiv preprint arXiv:1912.08165*, 2019. [17](#)
- S. Maji, J. Kannala, E. Rahtu, M. Blaschko, and A. Vedaldi. Fine-grained visual classification of aircraft. Technical report, 2013. [22](#), [23](#)
- Alex Nichol, Joshua Achiam, and John Schulman. On first-order meta-learning algorithms. *arXiv preprint arXiv:1803.02999*, 2018. [2](#)

- Maria-Elena Nilsback and Andrew Zisserman. Automated flower classification over a large number of classes. In *ICVGIP*, 2008. 22, 23
- Aude Oliva and Antonio Torralba. Modeling the shape of the scene: A holistic representation of the spatial envelope. *IJCV*, 2001. 1, 3
- Aaron van den Oord, Yazhe Li, and Oriol Vinyals. Representation learning with contrastive predictive coding. *arXiv preprint arXiv:1807.03748*, 2018. 5
- Maxime Oquab, Timothée Darcet, Théo Moutakanni, Huy Vo, Marc Szafraniec, Vasil Khalidov, Pierre Fernandez, Daniel Haziza, Francisco Massa, Alaaeldin El-Nouby, et al. Dinov2: Learning robust visual features without supervision. *TMLR*, 2023. 24
- Valentinos Pariza, Mohammadreza Salehi, and Yuki Asano. Hummingbird evaluation for vision encoders, 4 2024. URL <https://github.com/vpariza/open-hummingbird-eval>. 5
- Omkar M Parkhi, Andrea Vedaldi, Andrew Zisserman, and CV Jawahar. Cats and dogs. In *CVPR*, 2012. 22, 23
- F. Pedregosa, G. Varoquaux, A. Gramfort, V. Michel, B. Thirion, O. Grisel, M. Blondel, P. Prettenhofer, R. Weiss, V. Dubourg, J. Vanderplas, A. Passos, D. Cournapeau, M. Brucher, M. Perrot, and E. Duchesnay. Scikit-learn: Machine learning in Python. *JMLR*, 2011. 6
- Florent Perronnin, Jorge Sánchez, and Thomas Mensink. Improving the fisher kernel for large-scale image classification. In *ECCV*, 2010. 3
- James Philbin, Ondrej Chum, Michael Isard, Josef Sivic, and Andrew Zisserman. Object retrieval with large vocabularies and fast spatial matching. In *2007 IEEE conference on computer vision and pattern recognition*. IEEE, 2007. 16, 17
- James Philbin, Ondrej Chum, Michael Isard, Josef Sivic, and Andrew Zisserman. Lost in quantization: Improving particular object retrieval in large scale image databases. In *2008 IEEE conference on computer vision and pattern recognition*. IEEE, 2008. 16, 17
- Karol J. Piczak. ESC: Dataset for Environmental Sound Classification. In *Proceedings of the 23rd Annual ACM Conference on Multimedia*, pp. 1015–1018. ACM Press, 2015. ISBN 978-1-4503-3459-4. doi: 10.1145/2733373.2806390. URL <http://dl.acm.org/citation.cfm?doid=2733373.2806390>. 17, 23
- Filip Radenović, Ahmet Iscen, Giorgos Tolias, Yannis Avrithis, and Ondřej Chum. Revisiting oxford and paris: Large-scale image retrieval benchmarking. In *Proceedings of the IEEE conference on computer vision and pattern recognition*, 2018. 16
- Alec Radford, Jong Wook Kim, Chris Hallacy, Aditya Ramesh, Gabriel Goh, Sandhini Agarwal, Girish Sastry, Amanda Askell, Pamela Mishkin, Jack Clark, et al. Learning transferable visual models from natural language supervision. In *ICML*, 2021. 9, 16, 24
- Colin Raffel, Noam Shazeer, Adam Roberts, Katherine Lee, Sharan Narang, Michael Matena, Yanqi Zhou, Wei Li, and Peter J Liu. Exploring the limits of transfer learning with a unified text-to-text transformer. *JMLR*, 2020. 8, 24
- Olga Russakovsky, Jia Deng, Hao Su, Jonathan Krause, Sanjeev Satheesh, Sean Ma, Zhiheng Huang, Andrej Karpathy, Aditya Khosla, Michael Bernstein, et al. Imagenet large scale visual recognition challenge. *IJCV*, 2015. 22, 23
- Adam Santoro, Sergey Bartunov, Matthew Botvinick, Daan Wierstra, and Timothy Lillicrap. Meta-learning with memory-augmented neural networks. In *ICML*, 2016. 2
- Rico Sennrich, Barry Haddow, and Alexandra Birch. Improving neural machine translation models with monolingual data. In *ACL*, 2016. 8
- Oriane Siméoni, Gilles Puy, Huy V Vo, Simon Roburin, Spyros Gidaris, Andrei Bursuc, Patrick Pérez, Renaud Marlet, and Jean Ponce. Localizing objects with self-supervised transformers and no labels. In *BMVC*, 2021. 3

- Sivic and Zisserman. Video google: A text retrieval approach to object matching in videos. In *ICCV*, 2003. 1, 3
- Jake Snell, Kevin Swersky, and Richard Zemel. Prototypical networks for few-shot learning. *NeurIPS*, 30, 2017. 2
- Richard Socher, Alex Perelygin, Jean Wu, Jason Chuang, Christopher D. Manning, Andrew Ng, and Christopher Potts. Recursive deep models for semantic compositionality over a sentiment treebank. In *EMNLP*, 2013. 22, 23
- Andreas Steiner, Alexander Kolesnikov, Xiaohua Zhai, Ross Wightman, Jakob Uszkoreit, and Lucas Beyer. How to train your vit? data, augmentation, and regularization in vision transformers. *arXiv preprint arXiv:2106.10270*, 2021. 6, 7, 16, 19, 24
- Quan Sun, Yuxin Fang, Ledell Wu, Xinlong Wang, and Yue Cao. Eva-clip: Improved training techniques for clip at scale. *arXiv preprint arXiv:2303.15389*, 2023. 9, 16, 24
- Yu Sun, Xiaolong Wang, Zhuang Liu, John Miller, Alexei Efros, and Moritz Hardt. Test-time training with self-supervision for generalization under distribution shifts. In *ICML*, 2020. 3
- Giorgos Tolias, Yannis Avrithis, and Hervé Jégou. To aggregate or not to aggregate: Selective match kernels for image search. In *ICCV*, 2013. 3
- Antonio Torralba, Rob Fergus, and William T Freeman. 80 million tiny images: A large data set for nonparametric object and scene recognition. *TPAMI*, 2008. 1
- Hugo Touvron, Matthieu Cord, Matthijs Douze, Francisco Massa, Alexandre Sablayrolles, and Hervé Jégou. Training data-efficient image transformers & distillation through attention. In *ICML*. PMLR, 2021. 24
- Koen Van De Sande, Theo Gevers, and Cees Snoek. Evaluating color descriptors for object and scene recognition. *TPAMI*, 2009. 1
- Oriol Vinyals, Charles Blundell, Timothy Lillicrap, Daan Wierstra, et al. Matching networks for one shot learning. *NeurIPS*, 2016. 2
- Catherine Wah, Steve Branson, Peter Welinder, Pietro Perona, and Serge Belongie. The caltech-ucsd birds-200-2011 dataset. 2011. 22, 23
- Pete Warden. Speech commands: A dataset for limited-vocabulary speech recognition. *arXiv preprint arXiv:1804.03209*, 2018. 17, 23
- Ross Wightman. Pytorch image models. <https://github.com/rwightman/pytorch-image-models>, 2019. 6, 16, 24
- Thomas Wolf, Lysandre Debut, Victor Sanh, Julien Chaumond, Clement Delangue, Anthony Moi, Pierric Cistac, Tim Rault, Rémi Louf, Morgan Funtowicz, Joe Davison, Sam Shleifer, Patrick von Platen, Clara Ma, Yacine Jernite, Julien Plu, Canwen Xu, Teven Le Scao, Sylvain Gugger, Mariama Drame, Quentin Lhoest, and Alexander M. Rush. Transformers: State-of-the-art natural language processing. In *EMNLP*, 2020. 24
- Benfeng Xu, Quan Wang, Zhendong Mao, Yajuan Lyu, Qiaoqiao She, and Yongdong Zhang.  $k$  nn prompting: Beyond-context learning with calibration-free nearest neighbor inference. *arXiv preprint arXiv:2303.13824*, 2023. 3
- I Zeki Yalniz, Hervé Jégou, Kan Chen, Manohar Paluri, and Dhruv Mahajan. Billion-scale semi-supervised learning for image classification. *arXiv preprint arXiv:1905.00546*, 2019. 1
- Xiang Zhang, Junbo Jake Zhao, and Yann LeCun. Character-level convolutional networks for text classification. In *NeurIPS*, 2015. 23
- Yuanhan Zhang, Kaiyang Zhou, and Ziwei Liu. What makes good examples for visual in-context learning? In *NeurIPS*, 2023. 2

- Bolei Zhou, Hang Zhao, Xavier Puig, Sanja Fidler, Adela Barriuso, and Antonio Torralba. Scene parsing through ade20k dataset. In *Proceedings of the IEEE Conference on Computer Vision and Pattern Recognition*, 2017. [7](#)
- Bolei Zhou, Hang Zhao, Xavier Puig, Tete Xiao, Sanja Fidler, Adela Barriuso, and Antonio Torralba. Semantic understanding of scenes through the ade20k dataset. *International Journal of Computer Vision*, 127(3):302–321, 2019. [7](#)
- Jinghao Zhou, Chen Wei, Huiyu Wang, Wei Shen, Cihang Xie, Alan Yuille, and Tao Kong. ibot: Image bert pre-training with online tokenizer. In *ICLR*, 2022. [3](#), [18](#)

## A Additional Experimental Results

In this section we first illustrate additional results that solidify the findings discussed in the main paper, followed by evaluations of FUNGI in image retrieval, audio classification, linear classification of image features and a brief investigation of the performance of gradients from clustering and masked image modeling self-supervised objectives.

In Table 8, we report the performance of embeddings and FUNGI features for some additional backbones, including CLIP and EVA-CLIP models, for which, as explained in the main text, we experience diminishing returns as the pretraining dataset size grows. Moreover, for both models, the SimCLR loss does not produce predictive gradients, which we hypothesize is due to models being saturated to a contrastive loss, as they use a similar objective for pretraining.

In Table 9, we report the mean accuracy and one standard deviation (computed via `numpy.std`) across three seeds for a subset of our datasets, using a DeiT ViT-B/16 backbone, showing that the performance improvements of FUNGI are consistent across seeds.

In Figure 11 we evaluate the effectiveness of FUNGI across different ViT model sizes. The findings show that FUNGI improves the results for all three ViT models (ViT-S, ViT-B, and ViT-L), with the biggest improvements observed in the ViT-B model.

In Table 7, we report the performance of FUNGI for in-context retrieval-based semantic segmentation on ADE20K, and show that our method outperforms DINO across all memory bank sizes and is competitive against HummingBird.

Table 7: **FUNGI features improve in-context semantic segmentation on ADE20K.** We report the mIoU for retrieval-based semantic segmentation on ADE20K, comparing a DINO baseline against FUNGI features and the self-supervised HummingBird model. Results from Balazevic et al. (2024) are marked with ‡. We resize each image to  $512 \times 512$  and extract  $32^2 = 1024$  patch features.

Backbone	Features	Memory Bank Size		
		$1024 \times 10^2$	$1024 \times 10^3$	$1024 \times 10^4$
DINO ViT-S/16	Embeddings	11.4	14.5	17.0
DINO ViT-S/16	FUNGI	<b>16.1</b> †4.7	<b>20.0</b> †5.5	<b>22.3</b> †5.3
DINO ViT-B/16	Embeddings	14.5	18.3	20.8
DINO ViT-B/16	FUNGI	<b>19.2</b> †4.7	<b>23.5</b> †5.2	<b>25.2</b> †4.4
HummingBird ViT-B/16‡	Embeddings	-	-	<b>28.3</b>

Table 8: **Additional backbones.** Average accuracy of embeddings and FUNGI features in k-nearest neighbor classification across 11 datasets for CLIP (Radford et al., 2021; Sun et al., 2023), AugReg (Steiner et al., 2021) from timm (Wightman, 2019), and masked autoencoder (He et al., 2022) models. “K”, “D” and “S” stand for KL, DINO and SimCLR, respectively.

	EVA CLIP ViT-B/16	AugReg IN21K ViT-L/16	CLIP ViT-B/16	AugReg IN21K ViT-B/16	AugReg IN21K ViT-S/16	MAE ViT-B/16
<b>Full Dataset</b>						
Features	83.2	74.7	73.7	66.4	65.6	24.0
+ K	83.8 †0.6	75.0 †0.3	76.9 †3.2	67.1 †0.7	65.3 †0.3	44.4 †20.4
+ K + D	<b>84.1</b> †0.9	76.2 †1.5	<b>77.7</b> †4.0	68.6 †2.2	67.1 †1.5	<b>45.4</b> †21.4
+ K + D + S	83.4 †0.2	<b>76.5</b> †1.8	74.6 †0.9	<b>69.3</b> †2.9	<b>67.6</b> †2.0	38.8 †14.8
<b>Few Shot</b>						
Features	53.1	47.7	43.0	38.6	37.4	7.5
+ K	54.0 †0.9	48.3 †0.6	47.2 †4.2	40.2 †1.6	37.7 †0.3	18.5 †11.0
+ K + D	<b>54.1</b> †1.0	48.5 †0.8	<b>47.9</b> †4.9	40.3 †1.7	38.7 †1.3	<b>19.2</b> †11.7
+ K + D + S	53.7 †0.6	<b>50.2</b> †2.5	44.4 †1.4	<b>41.0</b> †2.4	<b>39.5</b> †2.1	14.0 †6.5

### A.1 Image Retrieval

We evaluate the performance of FUNGI features in image retrieval using the revisited (Radenović et al., 2018) Oxford (Philbin et al., 2007) and Paris (Philbin et al., 2008) landmarks datasets. We report the mean average precision (mAP) for both the medium (M) and hard (H) splits.

Table 9: **The performance of FUNGI is consistent across seeds.** Average accuracies in k-nearest neighbor classification and one standard deviation for FUNGI features on 8 datasets, measured across three seeds using a DeIT ViT-B/16 backbone. “K”, “D” and “S” stand for KL, DINO and SimCLR, respectively.

	Cars	CUB	DTD	ESAT	Pets	Food	FGVC	Flowers
Embeddings	32.3	56.0	58.6	90.7	90.8	60.5	23.5	56.9
+ K	33.5 ± 0.2	57.9 ± 0.1	60.4 ± 0.2	91.6 ± 0.2	91.3 ± 0.2	61.5 ± 0.1	22.9 ± 0.1	60.7 ± 0.6
+ K + D	36.2 ± 0.2	60.9 ± 0.2	63.1 ± 0.3	93.4 ± 0.1	91.8 ± 0.0	65.2 ± 0.2	24.2 ± 0.4	64.3 ± 0.5
+ K + D + S	<b>39.3 ± 0.3</b>	<b>63.6 ± 0.3</b>	<b>64.1 ± 0.2</b>	<b>95.0 ± 0.2</b>	<b>92.1 ± 0.2</b>	<b>67.3 ± 0.1</b>	<b>28.3 ± 0.6</b>	<b>69.3 ± 0.5</b>

For this task, we use FUNGI features built with DINO and KL gradients, as the SimCLR gradients did not result in good retrieval performance. The results are displayed in Table 10 and show that FUNGI features improve the retrieval abilities of all backbones, except DINOv2. Our method is particularly effective when applied on CLIP backbones: on the Paris hard split, we improve by 12.4% and 7.2% for CLIP and EVA-CLIP, respectively.

Table 10: **FUNGI improves image retrieval.** Mean average precision (mAP) of embeddings and FUNGI for retrieval on the Paris (Philbin et al., 2008) and Oxford (Philbin et al., 2007) landmarks datasets, for both medium (M) and hard (H) splits. “K” and “D” stand for KL and DINO, respectively.

	DINOv2 ViT-B/14		DINO ViT-B/16		CLIP ViT-B/16		EVA CLIP ViT-B/16		DeIT ViT-B/16	
	M	H	M	H	M	H	M	H	M	H
<b>Oxford</b>										
Embeddings	69.7	42.0	39.2	11.0	31.4	10.8	36.7	12.7	36.6	12.6
+ K	<b>70.4</b> ↑0.7	<b>42.6</b> ↑0.6	38.6 ↓0.6	11.6 ↑0.6	40.4 ↑9.0	14.5 ↑3.7	39.9 ↑3.2	13.9 ↑1.2	36.9 ↑0.3	12.6 ↑0.0
+ D	69.4 ↓0.3	41.2 ↓0.8	<b>40.4</b> ↑1.2	12.9 ↑1.9	41.4 ↑10.0	<b>15.3</b> ↑4.5	40.9 ↑4.2	14.8 ↑2.1	38.8 ↑2.2	12.7 ↑0.1
+ K + D	70.1 ↑0.4	42.0 ↑0.0	39.8 ↑0.6	<b>13.0</b> ↑2.0	<b>42.6</b> ↑11.2	14.7 ↑3.9	<b>41.2</b> ↑4.5	<b>14.9</b> ↑2.2	<b>39.1</b> ↑2.5	<b>12.8</b> ↑0.2
<b>Paris</b>										
Embeddings	<b>89.4</b>	<b>77.5</b>	63.8	37.6	64.6	40.4	69.8	46.7	63.0	37.2
+ K	88.7 ↓0.7	76.2 ↓1.3	64.5 ↑0.7	38.4 ↑0.8	74.7 ↑10.1	<b>52.8</b> ↑12.4	<b>75.2</b> ↑5.4	<b>53.9</b> ↑7.2	63.6 ↑0.6	37.7 ↑0.5
+ D	89.0 ↓0.4	76.2 ↓1.3	65.6 ↑1.8	39.0 ↑1.4	72.0 ↑7.4	47.8 ↑7.4	72.9 ↑3.1	50.2 ↑3.5	<b>65.7</b> ↑2.7	<b>40.2</b> ↑3.0
+ K + D	88.7 ↓0.7	75.9 ↓1.6	<b>65.8</b> ↑2.0	<b>39.5</b> ↑1.9	<b>75.1</b> ↑10.5	52.5 ↑12.1	74.9 ↑5.1	53.0 ↑6.3	65.6 ↑2.6	40.0 ↑2.8

## A.2 Audio Classification

We evaluate FUNGI on the audio modality using SSAST (Gong et al., 2021, 2022), a self-supervised audio spectrogram transformer trained for audio and speech classification, as the backbone. We construct FUNGI features using  $\nabla_{\text{KL}}$  and  $\nabla_{\text{SimCLR}}$ , and test their performance in k-nearest neighbor classification on ESC 50 (Piczak, 2015) and SpeechCommands V2 (Warden, 2018).

We use the same formulation as in the vision experiments for the  $\mathcal{L}_{\text{KL}}$  and  $\mathcal{L}_{\text{SimCLR}}$  objectives. However, for the latter, we obtain 16 views of the same clip by adding uniform noise following Gong et al. (2022). If we define the filter bank of an audio clip as  $c \in \mathbb{R}^{h,w}$ , the noise-augmented clip  $\hat{c}$  is computed as:

$$\hat{c} = c + \frac{x_1 \cdot x_2}{10} \quad x_1 \sim U(0, 1)^{h,w} \quad x_2 \sim U(0, 1). \quad (7)$$

Finally,  $\hat{c}$  is shifted by a factor sampled from a discrete uniform distribution  $U(-10, 10)$ . The complete list of hyperparameters used for the audio classification experiments is reported in Table 12.

The results are reported in Table 11, and show that FUNGI features built using  $\nabla_{\text{KL}}$  yield promising results, improving by up to 4.2% on the baseline. On the other hand, using  $\nabla_{\text{SimCLR}}$  does not consistently yield improvements. It rather often causes a performance drop when combined with  $\nabla_{\text{KL}}$ . As with text classification, further research is needed to determine the optimal self-supervised objectives and data augmentation to extract predictive gradients.

## A.3 Linear Classification of Image Features

We evaluate FUNGI features in logistic regression, using the implementation from the cyanure library (Mairal, 2019). We train each classifier for a maximum of 300 epochs (30 in the case of ImageNet-1K) using  $L_2$  regularization. For each dataset and feature combination (i.e., embeddings, embeddings +  $\nabla_{\text{KL}}$ , etc.), we pick the best regularization parameter between 5 linearly spaced values in the interval

Table 11: **FUNGI works for audio.** Top-1 accuracies in k-nearest neighbor audio classification of embeddings and FUNGI features obtained from a SSAST backbone (Gong et al., 2022, 2021). “K” and “S” stand for KL and SimCLR, respectively.

	ESC 50		SpeechCommands V2	
	Full	5-shot	Full	5-shot
Features	42.8	20.0	27.4	5.3
+ K	<b>47.0</b> $\uparrow 4.2$	<b>21.2</b> $\uparrow 1.2$	<b>29.9</b> $\uparrow 2.5$	<b>6.1</b> $\uparrow 0.8$
+ S	45.2 $\uparrow 2.5$	19.0 $\downarrow 1.0$	25.4 $\downarrow 2.0$	5.5 $\uparrow 0.2$
+ K + S	45.8 $\uparrow 3.0$	21.0 $\uparrow 1.0$	27.3 $\downarrow 0.1$	5.8 $\uparrow 0.5$

Table 12: **Audio classification experimental details.** Parameters used to extract audio encoder gradients for the  $\mathcal{L}_{\text{KL}}$  (left) and  $\mathcal{L}_{\text{SimCLR}}$  (right) objectives.

Parameter		Value	
Parameter	Value	Parameter	Value
Temperature	15	Positive Views	16
Projection Dim	768	Negative Views	2
		Projection Dim	768
		Negatives Batch Size	$64 \times 2$
		Temperature	0.07

$[5 \times 10^{-6}, 5 \times 10^{-4}]$  using the validation set. For datasets without a validation set, we generate one using an 80/20 stratified split. The final model is trained using the entire training dataset.

We report the results in Table 13 and Table 14 and find that, in linear classification, FUNGI features are most effective for backbones pretrained using a supervised objective. In contrast, self-supervised backbones do not benefit as much. This is especially evident for DINO and DINOv2, where FUNGI often yields worse results, especially in a few shot scenarios. Contrary to the k-nearest neighbor classification results, the best features combination is backbone specific. In Figure 9, we show that significant performance improvements can be achieved by picking the best feature combination for each backbone.

#### A.4 Additional Gradients

In this section, we study the performance of gradients obtained by two additional self-supervised objectives, DeepCluster (Caron et al., 2018) and iBOT (Zhou et al., 2022) in k-nearest neighbor classification on ImageNet-100, using a DeiT ViT-B/16 backbone. DeepCluster is a self-distillation and explicit clustering-based self-supervised method that alternates between clustering image features and training a model to predict cluster assignments. iBOT is an extension of DINO that combines image and patch-level objectives, the latter implemented as a latent-space masked image modeling (MIM) objective, where a learnable patch token replaces a subset of patches, and the model must reconstruct them.

The results are displayed in Figure 10, and show that the objectives used in this work achieve performances on par with the model embeddings, even surpassing them in the case of DINO. At the same time, iBOT and DeepCluster instead produce gradients with relatively poor predictive performance. For the former, a possible reason is that it incorporates a dense loss, whose gradients may not help to discriminate examples on the image level. Regarding DeepCluster, models pretrained using this strategy had worse performance in retrieval tasks compared to supervised pretraining (Caron et al., 2018), which may explain the poor retrieval abilities of its gradients.

#### A.5 Additional Ablations

**DINO data augmentation and head.** To maximize the signal-to-noise ratio, we only use local and global crops for the DINO data augmentation. We validate this choice empirically, and the results in Table 15 show that random crops produce more discriminative gradients compared to the standard data augmentation policy. Moreover, we also empirically validate the choice of using two

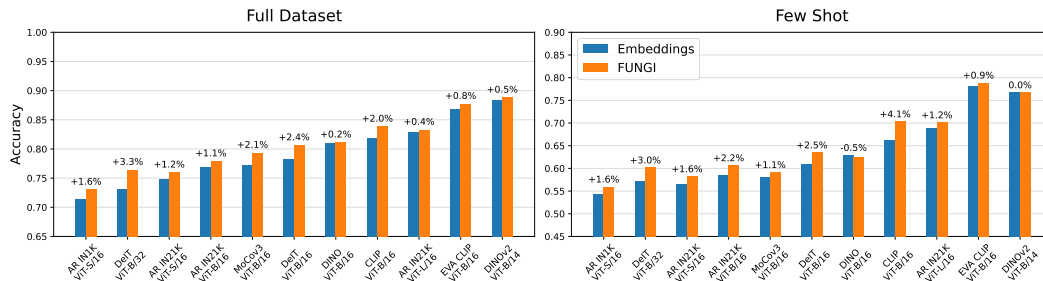


Figure 9: FUNGI works across backbones for linear probing. Accuracy in logistic regression-based image classification of embeddings and FUNGI features on various ViT backbones, both for full dataset and few shot setups, averaged over 11 datasets. For the FUNGI features, we chose the best performing combination across datasets. “AR” indicates AugReg backbones (Steiner et al., 2021).

Table 13: The best gradients for linear probing are backbone-specific for the main backbones. Average accuracy across 11 datasets for logistic regression-based image classification of embeddings and FUNGI features, constructed using multiple gradient combinations, for both standard and few shot setups using 7 backbones. “K”, “D” and “S” stand for KL, DINO and SimCLR, respectively.

	DINOv2 ViT-B/14	DINO ViT-B/16	DeiT ViT-B/16	MoCov3 ViT-B/32	DeiT ViT-B/32	AugReg IN1K ViT-B/16	AugReg IN1K ViT-S/16
<b>Full Dataset</b>							
Features	88.3	81.0	78.2	77.3	73.1	71.6	71.4
+ K	88.3 $\uparrow 0.0$	80.4 $\downarrow 0.6$	78.5 $\uparrow 0.3$	77.7 $\uparrow 0.4$	73.4 $\uparrow 0.3$	70.9 $\downarrow 0.7$	70.5 $\downarrow 0.9$
+ K + D	<b>88.8</b> $\uparrow 0.5$	<b>81.2</b> $\uparrow 0.2$	<b>80.7</b> $\uparrow 2.5$	<b>79.4</b> $\uparrow 2.1$	76.2 $\uparrow 3.1$	73.0 $\uparrow 1.4$	<b>73.0</b> $\uparrow 1.6$
+ K + D + S	88.7 $\uparrow 0.4$	80.7 $\downarrow 0.3$	80.5 $\uparrow 2.3$	78.7 $\uparrow 1.4$	<b>76.4</b> $\uparrow 3.3$	<b>73.1</b> $\uparrow 1.5$	<b>73.0</b> $\uparrow 1.6$
<b>Few Shot</b>							
Features	<b>76.7</b>	<b>62.9</b>	61.0	58.0	57.2	54.8	54.4
+ K	76.3 $\downarrow 0.4$	62.2 $\downarrow 0.7$	61.7 $\uparrow 0.7$	57.6 $\downarrow 0.4$	57.8 $\uparrow 0.6$	54.4 $\downarrow 0.4$	53.5 $\downarrow 0.9$
+ K + D	76.7 $\uparrow 0.0$	62.4 $\downarrow 0.5$	<b>63.5</b> $\uparrow 2.5$	<b>59.2</b> $\uparrow 1.2$	<b>60.2</b> $\uparrow 3.0$	56.5 $\uparrow 1.7$	55.9 $\uparrow 1.5$
+ K + D + S	76.6 $\downarrow 0.1$	61.6 $\downarrow 1.3$	63.4 $\uparrow 2.4$	58.7 $\uparrow 0.7$	60.1 $\uparrow 2.9$	<b>57.0</b> $\uparrow 2.2$	<b>56.0</b> $\uparrow 1.6$

independent heads for the DINO loss in Table 15, showing that this choice is beneficial for kNN classification.

**PCA.** We use Principal Component Analysis (PCA) to combine data from multiple losses at an iso-storage and retrieval speed cost. Given a dataset of FUNGI features, we fit the PCA on the training split and use it to transform both training and test splits. Table 16 lists the PCA dimensionalities used for each model architecture and shows that they do not cause a decrease in performance but rather provide a minor improvement.

## B Experimental Details

### B.1 Vision Nearest Neighbor Classification Experimental Details

**Hyperparameters.** We use three losses to extract gradients from vision backbones:  $\mathcal{L}_{\text{KL}}$ ,  $\mathcal{L}_{\text{DINO}}$  and  $\mathcal{L}_{\text{SimCLR}}$ . The exact parameters for each loss are shown in Table 17. This set of parameters is used consistently across backbones and datasets. While  $\mathcal{L}_{\text{KL}}$  and  $\mathcal{L}_{\text{DINO}}$  are robust to the choice of hyperparameters,  $\mathcal{L}_{\text{SimCLR}}$  is particularly sensitive to the number of positive views, as shown in Figure 12, where performance increases in a logarithmic fashion as more positive views are used, at the cost of gradient extraction speed. While this behavior is consistent across datasets, it has the most significant impact in datasets with many classes, e.g., Flowers102.

**SimCLR data augmentation and loss details.** Given an image, we patchify it in 49 overlapping views as follows: we first resize the input image to (224, 224), and then extract 49 patches of size  $112 \times 112$ , using a stride corresponding to  $1/6$  of the patch size. No other style or color augmentation is used. As the number of patches increases, so does the memory required to compute the loss and the

Table 14: **The best gradients for linear probing are backbone-specific for the additional backbones.** Average accuracy across 11 datasets for logistic regression-based image classification of embeddings and FUNGI features, constructed using multiple gradient combinations, for both standard and few shot setups using 6 backbones. “K”, “D” and “S” stand for KL, DINO and SimCLR, respectively.

	EVA CLIP ViT-B/16	AugReg IN21K ViT-L/16	CLIP ViT-B/16	AugReg IN21K ViT-B/16	AugReg IN21K ViT-S/16	MAE ViT-B/16
<b>Full Dataset</b>						
Features	86.9	82.9	81.8	76.8	75.6	38.6
+ K	87.2 $\uparrow$ 0.3	82.0 $\downarrow$ 0.9	82.6 $\uparrow$ 0.8	76.1 $\downarrow$ 0.7	74.4 $\downarrow$ 1.2	63.4 $\uparrow$ 24.8
+ K + D	<b>87.8</b> $\uparrow$ 0.9	<b>83.3</b> $\uparrow$ 0.4	<b>83.9</b> $\uparrow$ 2.1	<b>77.9</b> $\uparrow$ 1.1	76.6 $\uparrow$ 1.0	<b>66.2</b> $\uparrow$ 27.6
+ K + D + S	87.7 $\uparrow$ 0.8	83.2 $\uparrow$ 0.3	83.0 $\uparrow$ 1.2	77.8 $\uparrow$ 1.0	<b>76.8</b> $\uparrow$ 1.2	63.1 $\uparrow$ 24.5
<b>Few Shot</b>						
Features	78.0	68.9	66.2	58.4	57.6	23.9
+ K	78.6 $\uparrow$ 0.6	69.0 $\uparrow$ 0.1	69.3 $\uparrow$ 3.1	59.1 $\uparrow$ 0.7	57.6 $\uparrow$ 0.0	36.0 $\uparrow$ 12.1
+ K + D	<b>78.9</b> $\uparrow$ 0.9	<b>70.1</b> $\uparrow$ 1.2	<b>70.4</b> $\uparrow$ 4.2	<b>60.7</b> $\uparrow$ 2.3	<b>59.3</b> $\uparrow$ 1.7	<b>37.3</b> $\uparrow$ 13.4
+ K + D + S	77.5 $\downarrow$ 0.5	69.5 $\uparrow$ 0.6	65.9 $\downarrow$ 0.3	59.8 $\uparrow$ 1.4	58.6 $\uparrow$ 1.0	32.3 $\uparrow$ 8.4

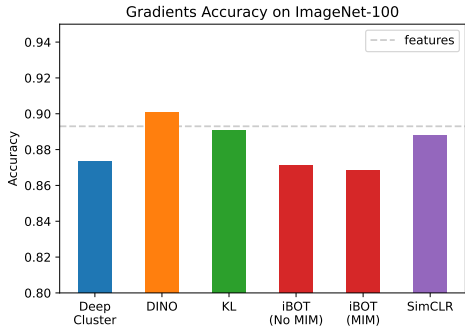


Figure 10: **Not all objectives produce good predictive gradients.** Top-1 accuracy in k-nearest neighbor classification of gradients obtained from different self-supervised objectives using a DeiT ViT-B/16 backbone. “MIM” stands for masked image modeling.

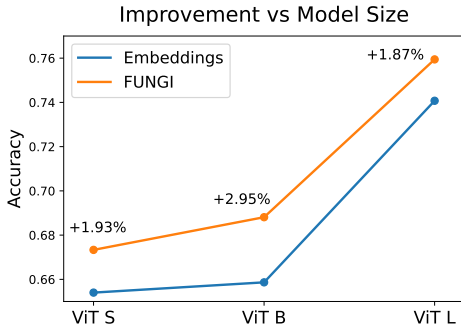


Figure 11: **Gains across backbone sizes.** Accuracy in k-nearest neighbor image classification averaged across 11 datasets using the model embeddings and FUNGI features extracted from AugReg backbones of increasing size.

gradients. This problem can be partially tackled by precomputing the negative batch, which in our experiments is picked randomly from the training dataset and kept constant for every input. Moreover, we can observe that the SimCLR loss is only defined for positive pairs, so we only need to compute the similarity of positive pairs to all other pairs, significantly reducing the size of the similarities matrix and memory usage.

## B.2 In-Context Scene Understanding Experimental Details

For the evaluation of the in-context scene understanding abilities of FUNGI features we closely replicate the setup described by Balazevic et al. (2024), and use the same parameters for both the full and few shot evaluations, with two minor exceptions: (1) we use a single augmentation epoch for the full dataset evaluation and (2) we use an anisotropic quantization threshold of 0.2 for the nearest neighbor index, as this parameter was not specified in the paper. The full set of parameters for the evaluation, loss computation and data augmentation is reported in Table 18. As for data augmentation, we use the same policy of Balazevic et al. (2024), and apply each augmentation independently.

In order to construct FUNGI features for this task, we implement a SimCLR loss that contrasts patch tokens from an input image to their nearest neighbors retrieved from a supporting memory bank. In practice, we:

Table 15: **DINO head configuration and data augmentation.** Top-1 accuracy on ImageNet-100 in k-nearest neighbor classification for the DINO gradients using shared or independent teacher and student heads (left) and with respect to the data augmentation policy (right).

Independent Heads	Accuracy	Data Augmentation	Accuracy
✗	88.4	DINO	88.9
✓	<b>89.1</b>	Random Crops	<b>90.1</b>

Table 16: **PCA does not degrade performance.** PCA output dimensionalities with respect to the backbone architecture (left) and its impact on k-nearest neighbor image classification accuracy averaged across 11 datasets using a DeiT ViT-B/16 backbone (right).

Architecture	PCA Dim		No PCA	PCA
ViT-S/16	384	Embeddings	65.1	65.3 $\uparrow 0.2$
ViT-B/16, ViT-L/16	512	+ KL	66.0	66.3 $\uparrow 0.3$
BERT, T5	512	+ KL + DINO	67.8	68.1 $\uparrow 0.3$
SSAST	512	+ KL + DINO + SimCLR	69.8	70.1 $\uparrow 0.3$

- Construct a memory bank of image patches of the same size as the one used for evaluation and its nearest neighbor index with ScaNN (Guo et al., 2020) following the procedure by Balazevic et al. (2024). We call this our support index.
- Then, for each image, we:
  1. Resize it to  $512 \times 512$ , compute its [CLS] and patch tokens and project them with a linear head. Excluding the [CLS] token, each image is mapped to  $32^2 = 1024$  features, as all our backbones use patches of size 16.
  2. For each token, retrieve its two nearest neighbors from the support index and randomly drop 50% of them.
  3. Compute the SimCLR loss, where the patch tokens constitute the positive set and the neighbors the negative batch. This allows us to compute a per-patch gradient.
  4. Drop the [CLS] token, as it does not correspond to a real image patch.
  5. Construct FUNGI features as in Equation 8, where  $f(x)$  maps an image to patches of dimension  $d$ ,  $L_2$  normalization is defined as  $z' = z/\|z\|_2$  and cat indicates concatenation.

$$F = \text{cat}'(\nabla' \mathcal{L}_{\text{SimCLR}}, f'(x)) \quad f(x) : \mathbb{R}^{3 \times 512 \times 512} \rightarrow \mathbb{R}^{1024 \times d} \quad (8)$$

### B.3 Text Classification Experimental Details

The parameters used to extract gradients from text encoders for  $\mathcal{L}_{\text{KL}}$  and  $\mathcal{L}_{\text{SimCLR}}$  are shown in Table 19. The gradient source layer is always the attention output projection of the last transformer

Table 17: **Image gradients setup.** Data augmentation and loss parameters used to extract gradients from vision encoders for  $\mathcal{L}_{\text{KL}}$ ,  $\mathcal{L}_{\text{SimCLR}}$  and  $\mathcal{L}_{\text{DINO}}$  (left to right).

Parameter	Value	Parameter	Value
Projection Dim	768	Projection Dim	96
Temperature	15	Neg. Batch	$256 \times 49$
		Temperature	0.07
		Parameter	Value
		Projection Dim	2048
		Global Crops	2
		Global Crop Scale	0.25, 1.0
		Global Crop Size	$224 \times 224$
		Local Crops	10
		Local Crop Scale	0.05, 0.25
		Local Crop Size	$224 \times 224$
		Teacher Temp.	0.07
		Student Temp.	0.1

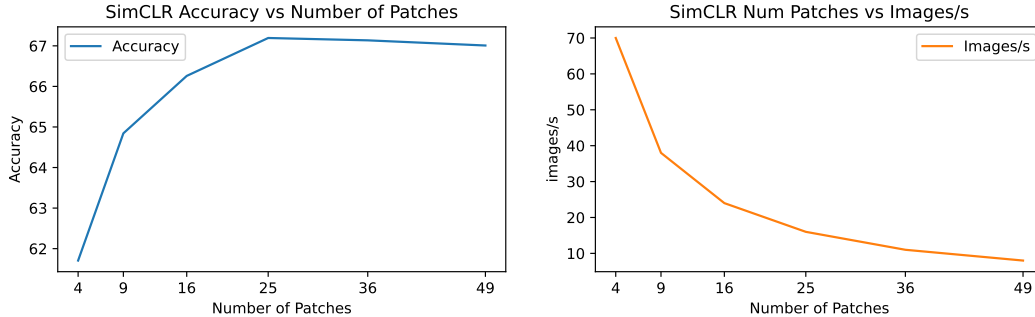


Figure 12: **SimCLR is sensitive to the number of views.** The SimCLR gradients mean-per-class accuracy on Flowers102 with respect to the number of patches (left) and the images/s versus the number of patches (right) using a supervised DeiT ViT-B/16 backbone.

Table 18: **In-context scene understanding setup.** Parameters (left) and data augmentation (right) used for the in-context scene understanding task for both full dataset and few shot setups. For the computation of  $\mathcal{L}_{\text{SimCLR}}$  we use 1025 views as we include the [CLS] token, which is discarded afterwards. The retrieved negatives indicate the number of neighbors retrieved from the support index, while the loss negatives the number of neighbors used for the loss computation. The color data augmentations are applied independently, in the order shown here.

Parameter	Full Dataset	Few-Shots
Memory Bank Size	See Table 3	$2048 \times 10^4$
Nearest Neighbors $k$	30	90
Temperature	0.02	0.1
Augmentation Epochs	1	8

ScaNN Index		
Num Leaves	512	512
Num Leaves to Search	32	256
Reordering Num Neighbors	120	1800
Dimensions per Block	4	4
Anisotropic Quantization	0.2	0.2

$\mathcal{L}_{\text{SimCLR}}$		
Support Index Size	See Table 3	$2048 \times 10^4$
Projection Dim	96	96
Positive Views	1025	1025
Negatives Batch Size	1025	1025
SimCLR Temperature	0.07	0.07
Retrieved Negatives per Patch	2	2
Loss Negatives per Patch	1	1

Parameter	Value
Random crop $p$	1.0
Scale factor	[0.5, 2.0]
Brightness jitter $p$	0.5
Contrast jitter $p$	0.5
Saturation jitter $p$	0.5
Hue jitter $p$	0.5
Max brightness $\Delta$	0.1
Max contrast $\Delta$	0.1
Max saturation $\Delta$	0.1
Max hue $\Delta$	0.1

encoder block. We use the same parameters across backbones. No data augmentation is used for the  $\mathcal{L}_{\text{KL}}$ , while for  $\mathcal{L}_{\text{SimCLR}}$  the views are obtained by randomly deleting words independently, where each word has a 10% probability of being deleted.

## C Data and Models

We investigate the performance of our gradient-enhanced features on 11 image classification datasets, namely CIFAR 10 and CIFAR 100 (Krizhevsky et al., 2009), Oxford Flowers 102 (Nilsback & Zisserman, 2008), Food101 (Bossard et al., 2014), ImageNet-1K (Russakovsky et al., 2015), FGVC Aircraft (Maji et al., 2013), CUB 200-2011 (Wah et al., 2011), Oxford-IIT Pets (Parkhi et al., 2012), Stanford Cars (Krause et al., 2013), DTD Textures (Cimpoi et al., 2014) and EuroSAT (Helber et al., 2019), 5 text classification datasets: TREC (Li & Roth, 2002) in its coarse version, banking-77 (Casanueva et al., 2020), Stanford Sentiment Treebank (SST) (Socher et al., 2013) in its fine-grained

Table 19: **Text classification experimental details.** Parameters used to extract text encoder gradients for the  $\mathcal{L}_{\text{KL}}$  (left) and  $\mathcal{L}_{\text{SimCLR}}$  (right) objectives.

Parameter	Value	Parameter	Value
		Positive Views	12
		Negative Views	2
Temperature	15	Projection Dim	256
Projection Dim	768	Negatives Batch Size	$256 \times 2$
		Temperature	0.07
		Word Deletion $p$	0.1

version, AG news (Zhang et al., 2015; Gulli, 2005) and tweet eval (emoji) (Barbieri et al., 2018, 2020) and 2 audio classification datasets: ESC 50 (Piczak, 2015), an environmental sound classification dataset, and SpeechCommands V2 (Warden, 2018), a keyword spotting task, where the goal is to classify utterances into a predefined set of words. The datasets, their license and citations are also listed in Table 20.

We follow the evaluation protocol for each individual dataset and report the top-1 accuracy for CIFAR 10 and 100, Food101, ImageNet-1K, Stanford Cars, EuroSAT, DTD Textures, CUB 200-2011, TREC, banking-77, SST, AG news, tweet eval (emoji), ESC 50 and SpeechCommands V2, and the mean-per-class accuracy for Flowers102, FGVC Aircraft and Oxford-IIT Pets.

We use the default splits defined by torchvision or the dataset authors where possible. As EuroSAT does not explicitly define a test split, we use an 80/20 stratified split as indicated by the dataset paper. We always report metrics on the test splits, with the exception of ImageNet, for which we use the validation split.

Table 20: **Datasets.** Summary table of all datasets used in this paper, their license and citation.

Dataset	Type	License	Citation
CIFAR 10	Image	Unknown	Krizhevsky et al. (2009)
CIFAR 100	Image	Unknown	Krizhevsky et al. (2009)
Stanford Cars	Image	Custom (Non Commercial)	Krause et al. (2013)
DTD Textures	Image	Custom (Research Only)	Cimpoi et al. (2014)
EuroSAT	Image	MIT	Helber et al. (2019)
CUB 200 (2011)	Image	Custom (Research Only, Non Commercial)	Wah et al. (2011)
Oxford-IIT Pets	Image	CC BY-SA 4.0	Parkhi et al. (2012)
Food101	Image	Unknown	Bossard et al. (2014)
FGVC Aircraft	Image	Custom (Research Only, Non Commercial)	Maji et al. (2013)
Flowers102	Image	Unknown	Nilsback & Zisserman (2008)
ImageNet 1K	Image	Custom (Research Only, Non Commercial)	Russakovsky et al. (2015)
ImageNet 100	Image	Custom (Research Only, Non Commercial)	Russakovsky et al. (2015)
TREC	Text	Unknown	Li & Roth (2002)
Banking-77	Text	CC BY 4.0	Casanueva et al. (2020)
SST	Text	Unknown	Socher et al. (2013)
AG News	Text	Custom (Non Commercial)	Zhang et al. (2015); Gulli (2005)
Tweet Eval	Text	Unknown	Barbieri et al. (2018, 2020)
ESC 50	Audio	CC BY-NC 3.0	Piczak (2015)
SpeechCommands V2	Audio	CC BY 4.0	Warden (2018)

We evaluate FUNGI features across several architectures, pretraining strategies and model sizes. These are listed in Table 21, alongside their license, data type and citation.

## D Compute Resources

All our experiments were run on a single NVIDIA A100 GPU with 40GB of VRAM. Considering the inference times listed in Table 22, replicating the k-nearest neighbor image classification results would require approximately 27 GPU hours per backbone using float16, which we use throughout all our experiments. As we evaluate our method across 13 backbones, reproducing these results would require 351 GPU hours. As for the text and audio classification experiments, they require around 3 GPU hours per backbone, for a total of 9 hours.

Table 21: **Models used in the paper.** Summary table of all architectures/pretraining strategies evaluated in the paper, along with their license, citation, and implementation, if applicable.

Model	Type	License	Citation
Masked Autoencoders	Image	CC BY-NC 4.0	He et al. (2022); Wightman (2019)
AugReg	Image	Apache 2.0	Steiner et al. (2021); Wightman (2019)
DeiT	Image	Apache 2.0	Touvron et al. (2021)
DINO	Image	Apache 2.0	Caron et al. (2021)
DINOv2	Image	Apache 2.0	Oquab et al. (2023)
CLIP	Image	MIT	Radford et al. (2021); Wightman (2019)
EVA-CLIP	Image	MIT	Sun et al. (2023); Wightman (2019)
MoCov3	Image	CC BY-NC 4.0	Chen et al. (2021)
BERT	Text	Apache 2.0	Devlin et al. (2018); Wolf et al. (2020)
T5	Text	Apache 2.0	Raffel et al. (2020); Wolf et al. (2020)
SSAST	Audio	BSD 3-Clause	Gong et al. (2022, 2021)

Table 22: **FUNGI introduces a speed overhead.** Embeddings and gradients extraction speed measured in images/second on an NVIDIA A100 GPU for a DeiT ViT-B/16 backbone. The gradients speed include the random projection step. The performance column reports the accuracy averaged across 11 datasets for the combination of a single gradient with the model embeddings. † indicates k-nearest neighbor inference on CPU.

Features Source	Images/s	Inference Speed (samples/s)†	Performance
Embeddings	479	2700	67.3
$\nabla_{\text{KL}}$	344	2700	68.2 †0.9
$\nabla_{\text{DINO}}$	32	2700	70.1 †2.8
$\nabla_{\text{SimCLR}}$	12	2700	70.9 †3.6

The in-context scene understanding experiments are relatively fast, requiring less than one GPU hour on average, resulting in an upper bound of 40 GPU hours.

Finally, our ablation studies required approximately 38 hours, while the preliminary experiments for this paper required a negligible amount of compute.

## E Algorithm

Algorithm 1 provides pytorch-style pseudocode for the computation of  $\mathcal{L}_{\text{KL}}$ , the gradient extraction, and the computation of FUNGI features (without PCA).

**Algorithm 1** PyTorch pseudocode for the KL FUNGI features.

```

# model, head: the vision backbone and the projection head
# feat_dim, grad_dim: the model features and gradients (as vectors) dimensionality
# projection: the random projection used to downsample gradients
projection = (torch.rand(feat_dim, grad_dim) - 0.5) > 0
uniform = torch.ones(feat_dim) / feat_dim

for x in dataset:
    # Extract the feature and its projection
    y = model(x)
    z = head(y)

    kl_div(log_softmax(z), softmax(uniform)).backward() # Calculate the loss and backpropagate
    layer = model.blocks.11.attn.proj # Select the target layer

    # Extract and project the gradients
    gradients = torch.cat([layer.weight.grad, layer.bias.grad.unsqueeze(dim=-1)], dim=-1)
    gradients = projection @ gradients.view(-1)

    y, gradients = normalize(y), normalize(gradients) # L2 normalize features and gradients independently

    feature = torch.cat([y, gradients], dim=-1) # Build the final feature

```